Large-Scale Redistributions of Atmospheric Mass

JOHN R. CHRISTY*

University of Illinois, Urbana, Illinois

KEVIN E. TRENBERTH

National Center for Atmospheric Research,† Boulder, Colorado

JOHN R. ANDERSON

University of Wisconsin, Madison, Wisconsin

(Manuscript received 6 May 1988, in final form 28 September 1988)

ABSTRACT

Seven years of daily global surface pressure (P_s) analyses derived from European Centre for Medium Range Forecasts (ECMWF) data are examined to describe more fully interhemispheric mass exchanges and intraseasonal variability. Extreme events in hemispheric mean P_s are determined, and composited grid point differences show that hemispheric anomalies are mainly determined by pressures in the North Pacific, western North Atlantic, northern Asia and the Southern Hemisphere (SH) circumpolar trough. Seasonal differences in the composites indicate that the regional anomalies occur farther poleward in the winter hemisphere, and the tropical anomalies tend to have the same sign as that of the summer hemispheric mean anomaly.

Long-lasting, localized, extreme P_s anomalies are identified in 18 significant events of hemispheric mass imbalance, and are found to be highly favored when the hemispheric mean departs significantly from normal. The result implies that regionally persistent anomalies are related to global-scale mass redistributions, rather than being totally the result of more localized redistributions.

The global atmospheric angular momentum exhibits significant changes during interhemispheric mass imbalances that exceed one standard deviation (about 0.4 mb). There is a strong tendency for the hemisphere in which a deficit of mass occurs to experience, on average, a 5% increase in hemispheric angular momentum.

Zonal complex empirical orthogonal functions are used to describe the $P_s \cos\phi$ anomalies, filtered for 30–75 day fluctuations. Dominant modes are found in which each hemisphere, independently, produced *intra*hemispheric exchanges between polar and temperate latitudes. An *inter*hemispheric mode indicates exchanges of mass between the midlatitudes of the Northern Hemisphere and the entire tropics plus the SH subtropics. The interhemispheric mode displays a southward propagation of anomalies from the tropical belt into the SH.

1. Introduction

The distribution of the mass of the atmosphere, given at the earth's surface by surface pressure (P_s), is a measure of the large-scale atmospheric circulation. Because P_s is essentially a vertically integrated quantity, it is affected by processes occurring above the surface. For example, relatively low P_s usually indicates positive thermal anomalies while relatively high P_s is associated with cooling and subsidence. Comparisons between the time-mean fields of mass and vertically integrated diabatic heating rates bear this out. Atmospheric cooling is found in places of high P_s, e.g. over oceanic highs and winter continents, while heating occurs in places of relatively low P_s, as seen over summer continents and tropical latitudes (Boer and Sargent 1985; Holopainen and Fortelius 1986; Chen and Baker 1986).

Slowly varying and large-scale redistributions in P_s are also useful indicators of flow anomalies produced in time-averaged solutions to diabatically forced global models. Some of these solutions have shown an equivalent barotropic response in the general circulation, especially in flow anomalies far from the source of the forcing (Blackmon et al. 1983; Geisler et al. 1985; Chen and Trenberth 1988). Large-scale barotropic responses in the atmosphere will have a signature in the P_s field by their very nature, and so knowledge of the variability in P_s may point to variability in atmospheric forcing.

The purpose of the present study is to report on large-scale redistributions of atmospheric mass found in daily

* Present affiliation: University of Alabama, Huntsville, Alabama.

† The National Center for Atmospheric Research is sponsored by the National Science Foundation.

Corresponding author address: Dr. John R. Christy, Atmospheric Science and Remote Sensing Laboratory, University of Alabama, Huntsville, Alabama 35899.

global analyses of P_s. Section 2 presents background material relevant to the paper and section 3 describes the data examined herein. Large-scale variability will be viewed from two perspectives. In section 4, the mass distribution associated with extreme events in interhemispheric mass imbalance will be examined. The second perspective is presented in section 5 in which the systematic redistribution of mass occurring in the 30–75 day period band is examined by means of complex empirical orthogonal function analysis. In both sections, the thrust is to determine the global-scale redistributions of atmospheric mass on intraseasonal time scales. A discussion and summary section concludes the work.

2. Background

Conservation of the global mass of dry air provides a useful constraint which can be employed to evaluate pressure analyses. On the hemispheric scale, Trenberth (1981) demonstrated that interhemispheric exchanges of mass occur in association with seasonal heating and cooling. The range of the interhemispheric exchange of mass is about 2 mb in the annual cycle of hemispheric mean P_s when pressure due to water vapor is removed. The hemispheric mean pressure is lowest in summer.

Significant interannual variations in hemispheric mean atmospheric mass have also been found and discussed in Trenberth (1984), Christy and Trenberth (1985) and Trenberth and Christy (1985a,b). In particular, the Southern Hemisphere (SH) circumpolar trough was shown to be especially deep from April to July 1979 during the Global Weather Experiment. This was verified by excessively greater than normal pressures over the Northern Hemisphere (NH) during this period. In fact, record high monthly values of NH mean sea-level pressure occurred in April and June 1979 in comparison to a reference period covering 58 yr.

Kutzbach and Guetter (1986) noted that the hemispheric mean sea level pressure of the NH during summer was significantly reduced in a simulation of the global atmosphere 9000 years ago. The result was obtained by providing the Community Climate Model at the National Center for Atmospheric Research (NCAR) with orbital parameters in effect at that time. The increase in solar radiation during NH summer, as compared with today, produced enhanced NH monsoon circulations, lower pressures over NH land (−2 mb), and higher pressures over NH oceans (+0.3 mb) with a net NH departure from present-day values of about −1 mb. This departure in NH mean pressure was attributed to a redistribution in mass caused by increased diabatic heating from solar radiation and latent heat release in the NH monsoon areas.

Other large-scale redistributions in atmospheric mass have been identified with respect to variations in the location of tropical heating anomalies. In the Southern Oscillation (SO), van Loon and Madden (1981) found a tendency for the tropical belt to experience greater than normal *zonal mean* pressures while the mid-latitudes of both hemispheres had negative mass anomalies during anomalous heating in the tropical Pacific. Barnett (1985) used gridded monthly normalized sea level pressures to show the two-dimensional redistribution of mass associated with the SO. It is clear from his work that the grid point anomalies in the tropical mass field are negatively correlated with anomalies in the diabatic heating field as indicated by precipitation amounts. Similarly, Madden and Julian (1972) discovered that in the 40–50 day tropical wave, zonal mean pressures in the tropics are anomalously high when convective anomalies peak in the western tropical Pacific.

Trenberth and Christy (1985a) were the first to utilize a global dataset to analyze the systematic redistributions of atmospheric mass (apart from the annual cycle) as represented by monthly zonal mean sea level pressure anomalies. Two modes of interest to the present topic were shown: 1) a symmetric mode in which anomalies in the tropics were negatively correlated with anomalies in midlatitudes of both hemispheres, and 2) an antisymmetric mode where anomalies in the midlatitudes of each hemisphere varied inversely. It was suggested that these mass redistributions occur as a result of large-scale thermal anomalies associated with tropical variations in heating and/or the variation in latent heating which accompanies shifts in midlatitude storm tracks.

With the planetary scale of the above mentioned processes becoming evident, a more detailed description of the redistributions which occur in the mass field should be made. It was partly due to the considerable work on the 40–50 day tropical wave and its signal found in the mass distribution (Madden and Julian 1972) that the present study concerns itself with intraseasonal time scales as presented by filtered *daily* P_s analyses. Monthly mean statistics cannot properly resolve fluctuations in this band.

3. Data

One of the major advantages in using 1000 mb heights and sea level pressure is their relatively robust nature, in that they are spatially coherent and insensitive to measurement site relocations. On the other hand, P_s is sensitive to relocations because of changes in topography. Analyses are derived by the two major operational centers: National Meteorological Center (NMC), and the European Centre for Medium Range Weather Forecasts (ECMWF) using a combination of model first-guess and direct measurements.

The analysis system at both centers undergoes continual revision and development in light of observational experience. This presents a problem for those engaged in climate analysis as it implies discontinuities

in the data archives (Trenberth et al. 1987). In particular, changes in surface orography in operational models produce spurious changes in P_s.

The ECMWF P_s data examined in this study were, therefore, derived from standard level geopotential height data and gridbox mean surface elevations, as described in Trenberth et al. (1987). The daily 0000 UTC analyses were interpolated to a rhomboidal wave-15 Gaussian grid (~4.4° lat by 7.5° long) which is roughly square at 55° lat. Data were examined for 1979–85 (December 1979 missing) except in section 4 where data were available for 1979–82 only. Because operational changes had little effect on the ECMWF 1000 mb height field and a prescribed orography was used, these derived ECMWF P_s data are consistent throughout the time period studied.

During the period of data available to us (1980–85), the archived NMC P_s analyses were affected by alterations in the representation of the earth's surface. In one instance, the global mean P_s dropped by 2 mb in the transition from grid point to spectral orography (Trenberth and Christy 1985a). This and other changes render the NMC P_s analyses of little value for detecting actual variations in quantities such as hemispheric mean P_s over periods longer than a few years. Trenberth and Olson (1988) have compared the global analyses from ECMWF and NMC. They conclude that fewer problems exist in the ECMWF data, and we therefore have chosen these data for our study.

The mean annual cycles of hemispheric and global mean ECMWF P_s are given in Fig. 1 for 1979–85. The greatest interhemispheric mass transport occurs in spring and fall. The amplitudes of the cycles are about 0.8 and 0.4 mb for the NH and SH respectively. The apparent lack of mass conservation in the global mean P_s is due to the annual cycle in global mean water vapor pressure which has a range of 0.4 mb. In Fig. 1, the global mean ranges from 983.3 to 983.7 mb. The variability of hemispheric mean P_s due to intraseasonal variations in water vapor pressure is at least one order of magnitude less than that of the total P_s (Trenberth et al. 1987). As such, anomalies from the annual cycle in hemispheric mean P_s are essentially those of the dry air only.

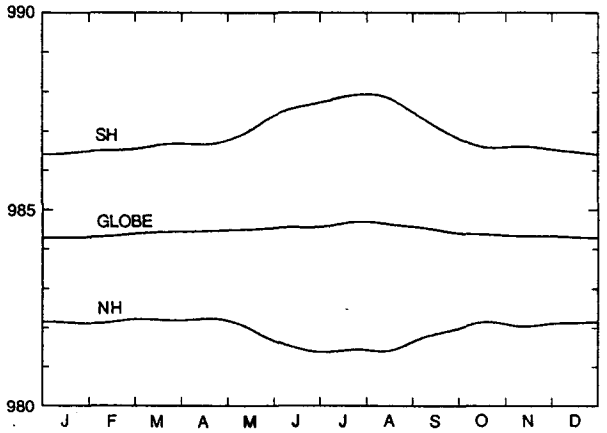

FIG. 1. Mean annual cycle of hemispheric mean P_s for SH (top), NH (bottom), and global mean P_s (middle) from ECMWF data for 1979–85 (mb).

Intraseasonal departures from this annual cycle can be quite large (Christy and Trenberth 1985; Trenberth and Christy 1985a). There have been several instances when the mean hemispheric P_s changed by more than 2 mb within a month. Figure 2 shows the filtered time series of the hemispheric mean P_s in which some of these cases are apparent in the upper panel (July 1979, February–March 1980, March 1981, October 1981 etc.). The filter is a tapered cosine designed with a "half-power" period of 41 days ($M = 20$ below):

$$x_i(\text{filtered}) = \sum_{j=-M}^{M} \left[\frac{1 + \cos\left(\frac{\pi j}{M + 0.5}\right)}{2M + 1} \right] x_{i+j}.$$

The zonal mean (brackets) departures from the mean annual cycle in $P_s \cos\phi$ for the 7-yr time series are also displayed in Fig. 2, filtered as in the hemispheric means above. The $\cos\phi$ factor provides an areal weighting so that net contributions to the hemispheric mean can be seen. Note that $[P_s] \cos\phi$ anomalies in the SH clearly have an intrahemispheric balance between polar and temperate latitudes (e.g., 1980). Positive equatorial mass anomalies are evident during early and late 1983, a year of a major El Nino–Southern Oscillation (ENSO) event. As has been mentioned, these positive anomalies are known to accompany ENSOs, and Trenberth and Christy (1985a) indicated that a portion (about 0.2 mb) of the tropical $[P_s] \cos\phi$ anomaly may be due to additional water vapor in the atmosphere.

Large interhemispheric exchanges in mass appear to have impact on regional climate. In early 1979, positive mass anomalies were seen in the NH midlatitudes and by June were visible in the tropics. The corresponding low values in the SH were reversed in July as an extreme positive anomaly developed near 50°S. In only two other periods (early 1982, mid-1984, Fig. 2) of the 7-yr time series do anomalies at that latitude approach the values of the 1979 event. Trenberth (1986) found that blocking episodes over the South Pacific east of New Zealand from late July to mid-September 1979 occurred in conjunction with the large influx of mass from the NH. From 13 July to 11 August, the SH mean P_s rose by over 1.7 mb, an amount which exceeds by a factor of 2 the normal range in the SH mean annual cycle. It seems that anomalous and persistent regional mass distributions may often be related to interhemispheric mass exchanges.

A spectral analysis of the time series of unfiltered NH mean P_s (annual cycle removed) is given in Fig. 3. The spectral estimates are calculated from a weighted

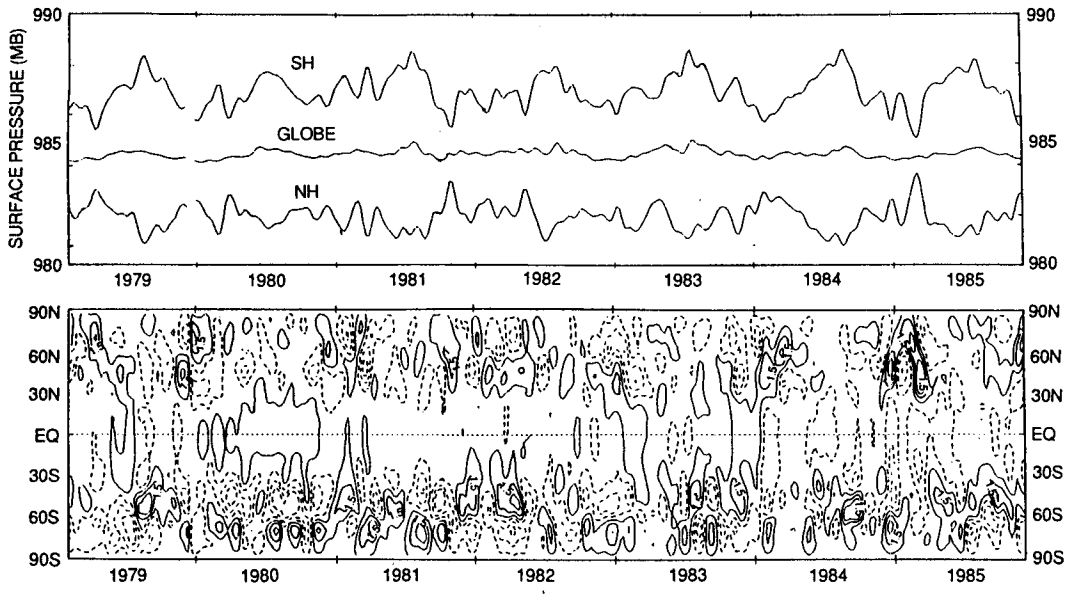

FIG. 2. Upper: Time series of filtered daily SH mean P_s (top), mean global P_s (middle), and NH mean P_s (bottom). Lower: departures from the mean annual cycle of filtered, $[P_s \cos\phi]$. Contour lines are 0.5, 1.5 and 2.5 mb. Dashed lines are negative departures.

Fourier transform of the truncated autocorrelation function. The weighting function is from Papoulus (1973) and produces 3.73 (N/M) degrees of freedom (N is sample size, and M is truncation point). In Fig. 3, $N = 2555$, $M = 260$, giving 37 degrees of freedom. The result is compared with a null hypothesis of red noise and reveals significant peaks at 40 and 64 day periods. Though some periods shorter than 20 days have significant values in the power spectrum, their total variance explained is an order of magnitude less than that which is found at periods 40 days and longer.

In section 4 we use these spectral results as a guide to determining the variability in the time series. Because most of the significant variance is in periods longer than 40 days, we select a reference period of 15 days centered on a day of a relative maximum or minimum in the NH P_s time series as an "event" used for further study. The data from which these events are identified is the time series of 15-day running mean NH P_s anomalies. A "significant" event will be an event whose value exceeds one standard deviation (0.43 mb) calculated from the same series. The background mean annual cycle from which these anomalies are produced is the mean daily NH P_s of the 1979–82 data which is smoothed by the tapered cosine filter described above with $M = 30$ (similar to Fig. 2). If an overlap occurs in adjacent significant events, only the event with the largest anomaly magnitude will be selected. Table 1 lists the events so chosen and the 15-day mean departure from the mean annual cycle. These events will form the set from which we will examine extreme interhemispheric mass imbalances.

For the complex empirical orthogonal function

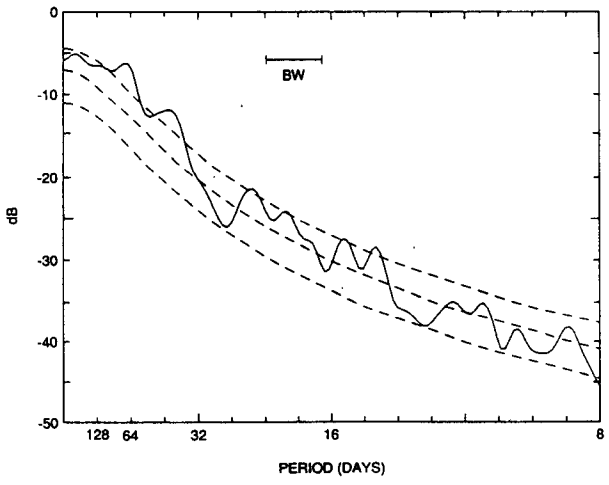

FIG. 3. Spectral analysis of unfiltered NH mean P_s with annual cycle removed. Dashed lines are (top) 95% significance level, (middle) red noise, and (bottom) 5% significance level. The sample size is 2555 with 37 degrees of freedom in the spectral calculation. The bandwidth (BW) is indicated.

TABLE 1. Dates and values of significant events in NH mean atmospheric mass (mb).

Negative		Positive	
Date	Value	Date	Value
14 Feb 1979	−0.49	14 Apr 1979	+0.80
11 Aug 1979	−0.93	13 Jul 1979	+0.48
2 Oct 1979	−1.05	5 Jan 1980	+0.51
26 Nov 1980	−1.01	18 Mar 1980	+0.88
21 Jan 1981	−0.87	28 Feb 1981	+0.80
22 Mar 1981	−1.39	25 Oct 1981	+1.61
13 May 1981	−0.77	4 Jan 1982	+0.56
6 Jun 1981	−0.89	2 Feb 1982	+0.80
19 Dec 1981	−0.50	9 Mar 1982	+1.21

analysis (section 5), we filter the daily data such that periods between 34 and 64 days have at least 90% of their power retained and periods between 30 and 75 days at least 50%. With such filtering, the two main peaks in the power spectrum at periods longer than 30 days are captured.

4. Extreme events

The events identified in section 3 are partitioned into two "seasons", December, January, February, and March (DJFM) and May–October (MY–OC) for compositing purposes. Because of the strong seasonality in the P_s distribution it is felt that events in one "season" are not directly comparable with events in the other "season" (Christy and Trenberth 1985). Note that there are five positive and five negative events in DJFM and four each in MY–OC.

a. Pressure

For each 15-day significant event, grid point P_s anomalies are determined. The background mean from which these anomalies are produced begins with a mean annual cycle of daily grid point averages of P_s taken from the 4-yr data record. Since there are only four values used for each daily grid point in this initial average, additional averaging is included by calculating the 45-day running mean of each grid point's mean annual cycle. As a result, each day's grid point mean P_s is determined from 180 data values.

These grid point anomalies (once the hemispheric mean P_s value is removed event by event) are composited for the high mass events from which are subtracted the composited anomalies of the low mass events. The results are depicted in Fig. 4 with stippling/shading to indicate grid point significance <5% when tested against a *t*-distribution with eight (six) degrees of freedom for DJFM (MY–OC). In both hemispheres and seasons, the area exceeding the 5% significance level is at least 16% of the total. The 4-yr database is too limited for rigorous field significance testing. Note, however, that for 500 mb maps, Lau and Phillips (1986) determined that when the area of local significance (estimated by a *t* test at 5%) exceeded 14%–15% of the total area, then the field as a whole was considered significant.

The pattern which emerges in Fig. 4 for DJFM NH is that anomalies in P_s over regions in the Gulf of Alaska, northeastern Canada and the northern rim of Asia are positively related to the sign of the anomaly in hemispheric mean P_s. With just as much significance, however, areas in the tropical Pacific and subtropical eastern Pacific and Atlantic are negatively correlated with NH mean P_s. The distribution of atmospheric mass for an average extreme hemispheric P_s event reveals some *intra*hemispheric compensation in NH winter. The results for DJFM in the SH are much more diffuse than in the NH. Areas equatorward of the circumpolar trough and in the central Pacific Ocean are seen to be positively related to the sign of the SH anomaly in P_s.

The differences in the composited anomalies of P_s for MY–OC are also given in Fig. 4. The distribution of anomaly differences in the NH (summer) is less compact compared with DJFM. Areas which are significantly (and positively) related to the hemispheric anomaly include southern Asia, the North Pacific, the North Atlantic and northeastern Canada. In the SH, the distribution of anomalies implies intrahemispheric mass compensation where anomalies in the circumpolar trough are partially balanced by anomalies in the tropical SH. The net result of this intrahemispheric imbalance is a hemispheric mean anomaly in P_s which carries the same sign as that near the circumpolar trough.

The inference in terms of $[P_s]$ in Fig. 4 is that mass anomalies in the winter hemisphere poleward of about 30° lat (25% of the global area) are offset by pressure anomalies throughout the tropics and summer midlatitudes. Inspection and subsequent testing of the individual patterns whose composites produced Fig. 4 showed that there were no local areas that were consistently (i.e., in every case) involved in the hemispheric anomalies. It did appear, however, that localized extreme anomalies were present somewhere. To test this notion, an experiment was designed to determine whether localized extreme anomalies (LEAs) in the individual 15-day mean 1000 mb geopotential height fields occur with any preference during significant events in hemispheric mean P_s. An LEA will be defined as a combination of values representing the areal extent of a contiguous region in which all 1000 mb grid point anomalies are found to exceed a series of prescribed thresholds of geopotential height. For a given significant event (Table 1) there may be several such areas in both hemispheres.

The procedure for quantifying the LEAs is to calculate the grid point anomalies of 1000 mb geopotential height for each event listed in Table 1. Then, in order not to bias the results, the hemispheric mean 1000 mb height is removed from the gridded anomalies. The magnitude of the LEA is calculated as an index (I) from the gridded anomalies:

$$I+ = (\text{area} > 75\ \text{gpm}) + (\text{area} > 100\ \text{gpm}) + \cdots + (\text{area} > 175\ \text{gpm})$$

$$I- = (\text{area} < 75\ \text{gpm}) + (\text{area} < 100\ \text{gpm}) + \cdots + (\text{area} < 175\ \text{gpm})$$

The index is scaled so that individual LEAs show a range in values of 0.2 to 50. The total number of contiguous regions with at least one grid point departure of 75 gpm in DJFM is 70, and 58 for MY–OC. The mean value of the LEAs is 4.5. The index is essentially

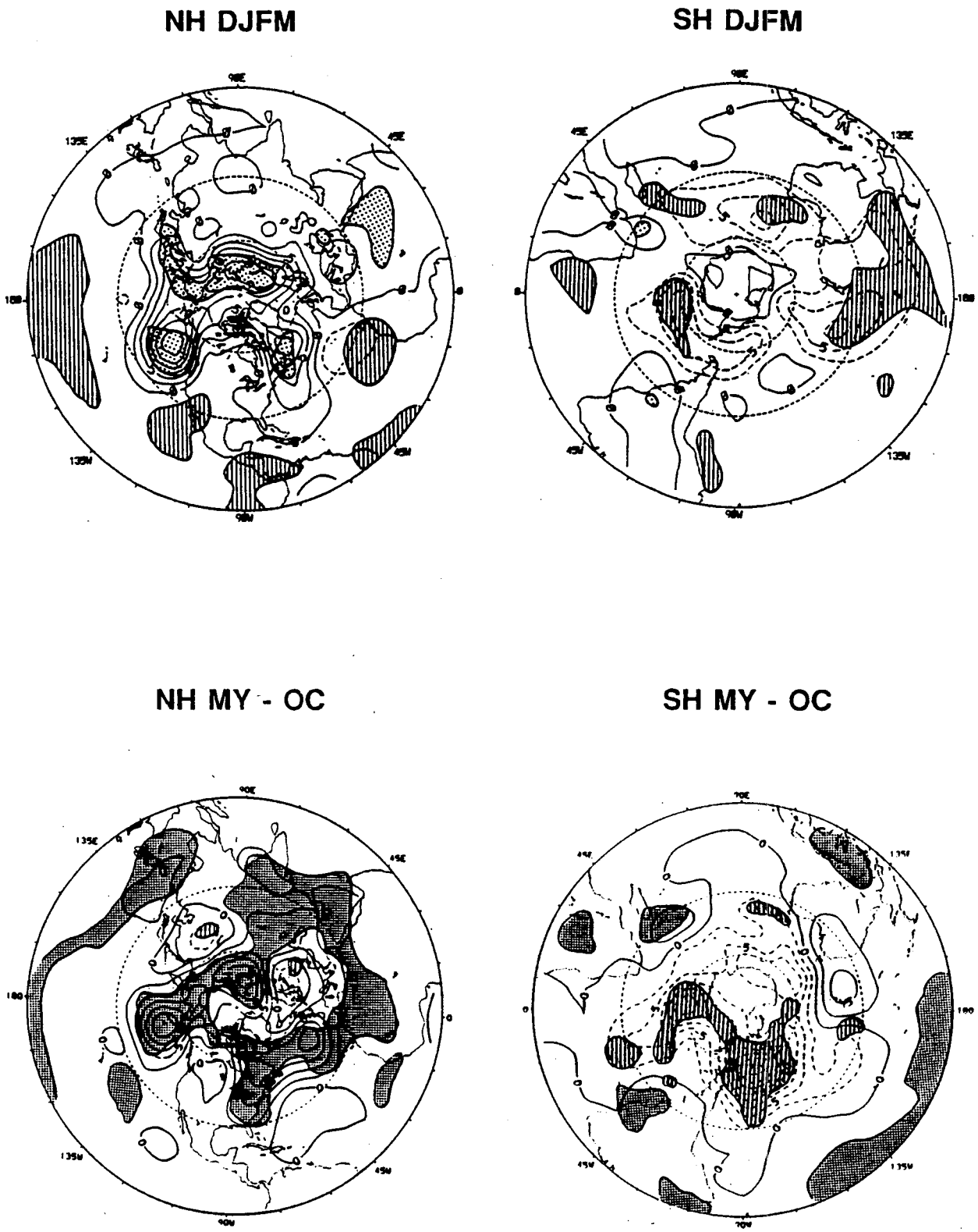

FIG. 4. Differences between composited anomalies of P_s (mb) of the NH high mass events minus the low mass events (see text) for DJFM (upper two) and MY–OC (lower two). Stippled areas are those in which the grid point value falls outside of the 95% confidence interval.

a measure of the amount of mass in the LEA. The statistic we examine is the sum of the indices partitioned according to hemispheric mass anomaly and "season." The results are shown in Table 2.

The method of determining significance in these results is by means of the chi-squared test applied to each subtable which has one degree of freedom. Both NH subtables and the MY–OC SH subtable are highly significant (<0.5%) meaning that localized extreme anomalies occur in conjunction with the hemispheric anomaly of the same sign. This is true for both hemispheres in "winter" and the NH's "summer." The SH "summer" showed no preference at all. The results indicate that the *global* mass distribution is significantly related to extreme *regional* anomalies, except in the SH during its "summer." In other words, localized, persistent features in the surface mass distribution typically occur in conjunction with cross-equatorial mass fluxes. This result was found to be evident in one case of SH blocking studied by Trenberth (1986).

b. Zonal wind

To relate a simple dynamical consequence of the anomalous mass distributions associated with extreme events in hemispheric mean P_s, one might expect that altered gradients in this field would leave their signature in the winds. For example, when hemispheric P_s is low in the winter hemisphere, the meridional gradients of P_s near 30° are on average enhanced (Fig. 4), implying increased westerlies.

The multilevel ECMWF zonal winds (u) are utilized to calculate global (M_G) and hemispheric (M_H) angular momentum of the atmosphere. This is done for each of the significant events listed in Table 1 and compared with background mean values calculated from the 4 yr of data available at that time.

$$M_G = \frac{2\pi a^3}{g} \int_{50\text{ mb}}^{P_s} \int_{-\pi/2}^{\pi/2} [u] \cos^2\phi d\phi dp.$$

The vertical integration incorporates P_s as the lower boundary. Anderson and Rosen (1983) and Rosen and Salstein (1983) utilized zonal winds "analyzed" from 1000 to 100 mb in NMC data, even though a large portion of the 1000 mb pressure surface was below the earth's surface. Rosen and Salstein report in a separate calculation using P_s for the lower boundary that the global result was affected by only 1% with virtually no impact on the variability of M_G with time.

The DJF mean M_G determined by Rosen and Salstein was about 1.6×10^{26} kg m^2 s^{-1}. The background mean values for M_G and M_H in our study are calculated from three consecutive half monthly periods over the 4 yr of data. For example, the background mean for the second half of December utilizes the data from 1 December through 15 January. The values of M_G for the five consecutive half-monthly periods from the last half of December through the second half of February are ($\times 10^{26}$ kg m^2 s^{-1}) 1.68, 1.67, 1.65, 1.62 and 1.59. For the first half of each of the months from May through August we calculated the mean values of M_G to be 1.62, 1.43, 1.18 and 1.11.

Anomalies in global atmospheric angular momentum (M'_G) were calculated for each of the 18 significant events in hemispheric mean P_s. The mean M'_G is 3.414×10^{24} kg m^2 s^{-1} [standard deviation (sd) = 7.506×10^{24} kg m^2 s^{-1}]. This is highly significant (<0.1%) and indicates that M_G tends to have positive anomalies during significant events in hemispheric mass imbalances.

Anomalies of M_H (M'_H, in units of 10^{24} kg m^2 s^{-1}) for all 18 selected events were also calculated. The pattern which emerges is the strong tendency for M_H to be greater than normal when the hemisphere has a deficit in mass. For low mass in the SH, the mean M'_{SH} is +4.71 (sd = 4.01). The same calculation for low mass in the NH indicates the average M'_{NH} is +3.83 (sd = 4.74). When the values for the 18 low mass hemispheres are taken together, the mean M'_H is +4.27 (sd = 4.41) which is significant (relative to a null hypothesis of $M'_H = 0$) at <0.01%.

Similar calculations of M'_H for the hemisphere with excessive mass in the 18 significant events are less revealing. The mean M'_{NH} is −1.02 (sd = 6.09) and for M'_{SH}, −0.67 (sd = 4.74). For all 18 events, the mean M'_H is −0.82 (sd = 4.94) which is not statistically significant.

It appears, therefore, that the global anomaly in angular momentum during extreme events in hemispheric mean P_s is due to the anomaly of M_H in the hemisphere with a deficit of mass. The value of M_H in the hemisphere with a surfeit of mass is inconsequential to the global calculation.

TABLE 2. The sum of the LEA statistic partitioned according to hemisphere, hemispheric mean P_s anomaly, and "season".

P_s anom	LEA anomaly I+	LEA anomaly I−	P_s anom	LEA anomaly I+	LEA anomaly I−
		DJFM			
+NH	96.0	43.6	+SH	39.9	26.3
−NH	40.5	68.4	−SH	52.4	15.5
		MY-OC			
+NH	17.3	0.4	+SH	50.9	21.3
−NH	4.1	15.1	−SH	14.8	94.8

5. Systematic redistributions of atmospheric mass

Section 4 dealt with the distribution of mass during events of significant departures from normal of hemispheric mean P_s. An examination of Fig. 2 indicates that interhemispheric exchanges of mass occur with

regularity. To identify the more common modes of mass redistribution we shall use the frequently employed technique of empirical orthogonal functions (EOFs) using the zonal mean P_s values derived from the ECMWF data.

The first EOF calculation utilizes the daily anomalies in $[P_s]\cos\phi$ and is given in Fig. 5. Intrahemispheric SH mass exchange is depicted in EOF 1, while mass exchanges between the higher latitudes and a broad tropical-subtropical region are revealed in EOFs 2 and 4. A combination of interhemispheric and NH-intrahemispheric mass exchange is seen in EOF 3. The variances explained by these first four EOFs are respectively 42%, 20%, 16%, and 12%. All EOFs here and throughout this section are separable according to the criterion of North et al. (1982).

These standard EOFs describe only coincidental relationships in the anomaly field. We know that large-scale mass anomalies appear in midlatitudes, but we do not know whether they propagate from other regions or develop in place. A complex EOF (CEOF) analysis allows for the identification of propagating and phase-shifted relationships in the anomaly field. The method employed here follows that of Anderson and Rosen (1983), in which two filters are applied to the data, generating two time series for each point. The filters are designed to be orthogonal in time with respect to each other for a particular frequency band. In this way, for each spatial point there are two values, one at "zero" phase and one at "90°" phase. The EOF is then calculated for both time series simultaneously. In the present case, the filters allow the period band 30–75 days to be examined. The CEOFs for the $[P_s]\cos\phi$ anomalies are calculated for 1980–85, because December 1979 is missing.

Summed over all latitudes, the mean daily variance of the $[P_s]\cos\phi$ anomalies is 110.3 mb^2. The zonal distribution of this variance is given in Fig. 6 as well as the variance passed by the mean annual cycle (A) and by the 30–75 day filter (F). Most of the variance filtered out of the zonal anomalies is in periods less than 30 days, which have very little impact on interhemispheric mass exchange. The amount of variance passed by the filter is about 13% of the total and 21% of that apart from the mean annual cycle.

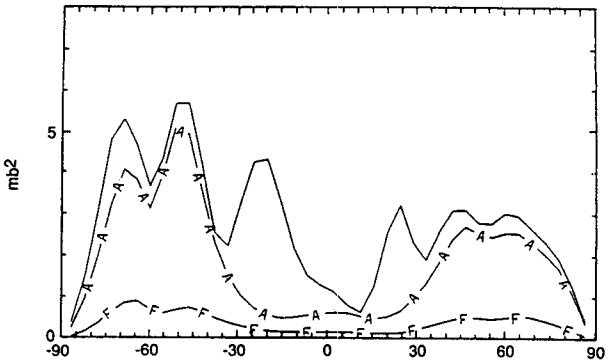

FIG. 6. Mean daily variance of P_s anomalies weighted by cosine of the latitude (top curve, mb^2). Curve (A) is the variance not associated with the annual cycle and curve (F) is the variance passed by the 30–75 day band-pass filter.

The first three zonal CEOFs (ZCs) are shown in order in Figs. 7–9. The modes explain 36%, 22%, and 15% of the filtered variance, respectively. The lower left panel of each diagram is a representation of 1 cycle (about 50 days) of the ZC anomalies. The lower right panel depicts the vertically integrated zonal mean meridional velocity required to accommodate the $[P_s]\cos\phi$ anomalies in a particular ZC of average amplitude. The velocity is that required by conservation of mass. In both lower panels, time is along the horizontal axis and latitude along the vertical. The three time series in the upper panel are, from top to bottom, the reconstructed NH mean P_s anomaly produced by the ZC, the ZC amplitude, and the ZC phase.

The first zonal CEOF (ZC 1) (Fig. 7) portrays the intrahemispheric mass exchange which occurs in the SH across about 55°S in a standing pattern. Virtually no interhemispheric mass exchange occurs in this mode as can be seen in the time series of the reconstructed NH P_s anomaly. The time series of the amplitude of ZC 1 shows no obvious seasonality. The mass is depicted as shifting between the two main centers of action (lower right).

In ZC 2 (Fig. 8), interhemispheric mass exchange is clearly evident. Though explaining only about 3% of the *total* unfiltered variance, it produces anomalies in NH mean P_s with a range of over 1 mb. The pattern shows a large anomaly centered at 50°N balanced by a broadly distributed anomaly in the tropics which extends into the SH. The tropical anomaly is depicted as "leading" the NH anomaly by a few days. The anomaly in the SH near 50°S peaks at ¼ cycle (about 13 days) after the maximum in the tropics, and appears to be

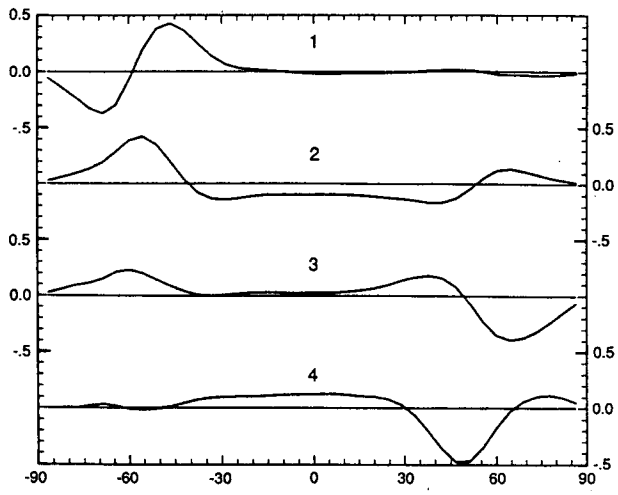

FIG. 5. The first four standard EOFs of $[P_s]\cos\phi$.

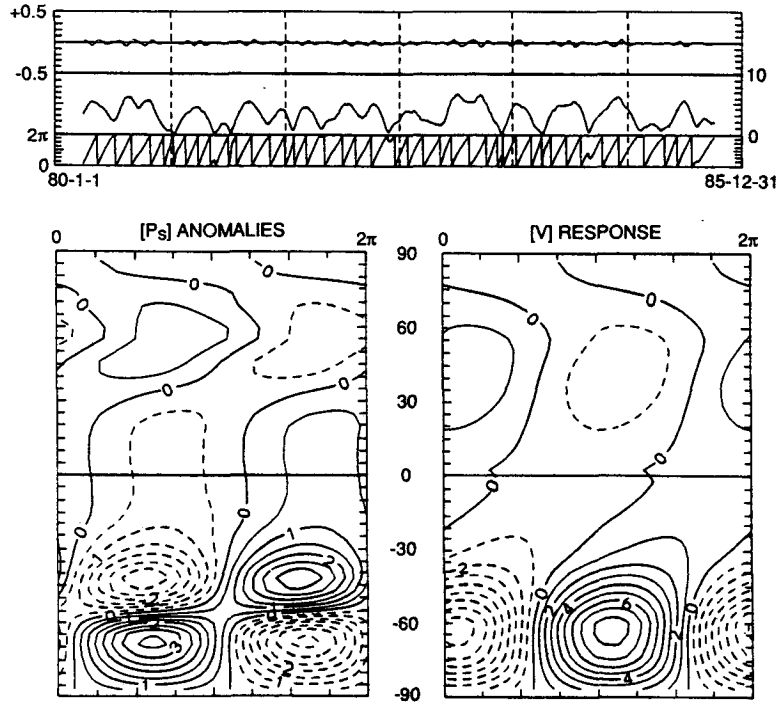

FIG. 7. Lower left: ZC 1 represented as a latitude-time cross section with period of roughly 50 days of zonal anomalies in $[P_s]\cos\phi$. Coefficients have been scaled to be larger than actual by a factor of 10. Lower right: associated vertically integrated zonal mean mass velocity of a ZC of average amplitude (contour interval is 1 mm s^{-1}). Top: time series of reconstructed NH P_s anomaly (top, mb), time series of ZC amplitude (middle) and time series of ZC phase (lower).

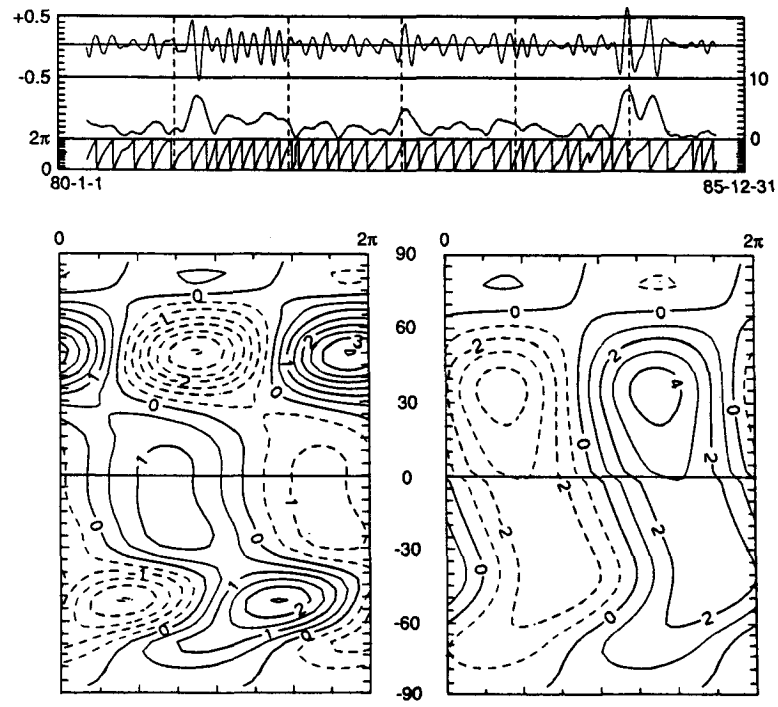

FIG. 8. As in Fig. 7, but for ZC 2.

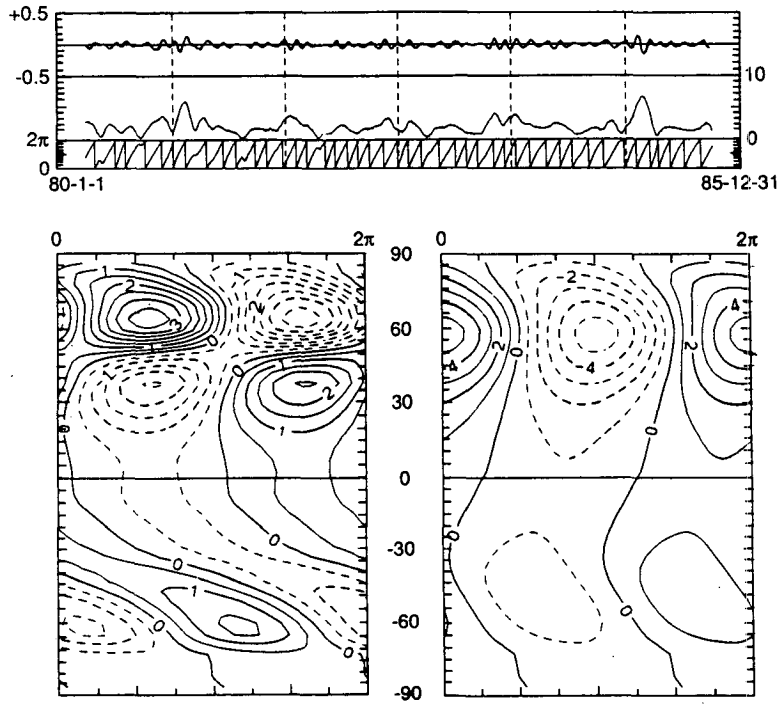

FIG. 9. As in Fig. 7, but for ZC 3.

at a point of convergence between anomalies propagating from the tropics southward and those moving from Antarctica northward. The mass field is shown to shift in virtual unison from 60°N to the SH with some southward displacement through time.

The time series of the amplitude of ZC 2 shows considerable interannual variability. The largest amplitudes are generally seen in the NH winter (e.g., 1984–85), yet in 1981 this mode was almost continually active. Other work (Anderson, 1988) has shown that 1981 was a very high amplitude year for the tropical 40–50 day wind oscillation, indicating a possible correspondence between ZC 2 and the well-known Madden–Julian oscillation (Madden and Julian 1972).

The third zonal CEOF (ZC 3) (Fig. 9) bears some resemblance to ZC 1 in that there is a large intrahemispheric exchange of mass but this time within the NH. There is a slight indication of anomaly propagation from the NH subtropics to the SH midlatitudes, but the coefficients in this feature are rather small in magnitude. Virtually no interhemispheric mass exchange is evident in ZC 3. The amplitude time series indicates that this mode appears mainly in the NH winter.

The global fluctuations in $[P_s]\cos\phi$ are evident in three major modes, two being *intra*hemispheric and the other, *inter*hemispheric. The SH intrahemispheric mode (ZC 1) is the dominant pattern in the global data and is active year round. The interhemispheric mode (ZC 2) actually accounts for more global variance than does the NH intrahemispheric mode (ZC 3) which is primarily evident in NH winter. The interhemispheric mode indicates a tendency for southward propagation of the tropical anomalies.

6. Discussion and summary

Several investigations have led to the discovery of preferred distributions of anomalies in atmospheric mass (Defant 1924; Walker and Bliss 1932; Lorenz 1951, etc.) The SO is viewed as depicting mass anomalies which "oscillate" between the eastern tropical SH Pacific and the Maritime continent (e.g., Barnett 1985). Other "oscillations" which have regional impact are the North Atlantic Oscillation (van Loon and Rogers 1978), Pacific/North American (Wallace and Gutzler 1981), and the 40–50 day tropical oscillation (Madden and Julian 1972). Usually, departures from monthly means are used as the data source in the midlatitude oscillations (and SO), but we have shown that for very large scale redistributions, it is desirable to have data with greater time sampling so as to resolve periods down to 30 days.

The analysis of the composited anomalies (Fig. 4) brings to light the interplay between hemispheric and regional scales. Though the composites were selected only on the basis of the hemispheric anomaly in P_s, they show that certain regions are highly correlated with the hemispheric mean. In particular, the North

Pacific, North Atlantic, northern Asia areas and, in the SH, the circumpolar trough were consistently involved in interhemispheric mass exchange. These anomalous regions were broad, however, and varied considerably from event to event.

The examination of localized extreme anomalies demonstrated again that the hemispheric mass anomaly tends to accumulate in relatively small areas. The point we wish to emphasize is that the existence of the persistent anomalies is to a significant degree related to cross-equatorial mass fluxes. Without these interhemispheric mass exchanges, the anomalies evidently could not attain their extreme values. Such a consideration must be incorporated into studies of persistent anomalies, such as blocking. That is to say, interhemispheric mass imbalances have repercussions for the localized distribution of mass.

In the calculation of angular momentum, we demonstrated that there was dynamical consistency between the enhanced gradients of $[P_s]$ and the zonal winds for the hemisphere with a mass deficit. There is normally a zonal gradient between the subtropical belt (high P_s) and the midlatitudes (lower P_s). During low mass events, this gradient is increased, on average, as was implied in the grid point anomalies (Fig. 4) and explicitly evident in ZC 2. The corresponding enhanced winds suggest an equivalent barotropic nature to the large-scale P_s anomalies. However, no such dynamical result was discovered for the opposite hemisphere in which there was a surplus of mass, and for which the $[P_s]$ gradients were not systematically affected.

The magnitude of the hemispheric momentum anomalies was about 5% (for NH winter and SH all year) of the total, while the hemispheric mass departures represented only 0.1% of the whole. This implies the changes in M_H were a dynamical response associated with the redistributed mass rather than the mechanical response of seeking to conserve M_H due to the loss (gain) in mass. Further research will address the question of the relationship between the general circulation and these interhemispheric mass imbalances. We suggest that the enhanced M_H in a hemisphere of relatively low P_s may be due to the strength of the subtropical and midlatitude jets, and therefore is related to the location of storm tracks.

The interhemispheric mass imbalance associated with the NH anomalies is compensated in the NH tropics (ZC 2) and the SH. An interesting feature found in ZC 2 was the southward propagation of tropical anomalies to the SH, while the NH anomalies appeared to be stationary relative to the tropics. This suggests that in one mode of atmospheric variability, the mass redistribution may be forced by some tropical NH interaction, which then moves into the SH.

In the SH, the dominant mode of mass redistribution is between polar and temperate latitudes in a basically zonal configuration (ZC 1). Rogers and van Loon (1982) examined this mode in more detail and found it to be a regular feature of the SH circulation. They also studied its vertical structure and determined it to be highly equivalent barotropic. Kidson (1986) examined the circulation during the SH winter of 1979 and reported an oscillating zonal index (45.75° vs 67.5°) in the 500 mb winds with a mean period of 27 days. The temperature variability in the oscillation was essentially homogeneous below 300 mb, and there was only a slight indication of changes in the net poleward heat flux between extremes in the cycle. So, again, the oscillation is primarily equivalent barotropic so that knowledge of the surface mass distribution is instructive as to SH circulation variability.

What also remains to be done is to relate the mass circulations in the tropics with the thermodynamic forcing. We noted that a "lead" indicator of interhemispheric mass exchanges may be the tropical mass anomalies (ZC 2). A thorough examination of the tropical budgets of mass, momentum and energy may identify the mechanisms by which a hemisphere experiences a net loss of atmospheric mass while undergoing an enhancement of angular momentum.

Acknowledgments. This research is supported by the National Science Foundation under Grant ATM-8516541, and forms part of the work contained in the first author's PhD thesis. We are pleased to acknowledge that the data analyzed in this study were provided by ECMWF. Appreciation is expressed to David England (UAH) for his assistance in preparing the manuscript.

REFERENCES

Anderson, J. R., 1988: A diagnostic study of the tropical 40–50 day oscillation. *Proc. 11th Annual Climate Diagnostics Workshop,* Champaign, U.S. Govt. Printing Office, Washington DC, 267–270 [NTIS PB87-175741].

——, and R. D. Rosen, 1983: The latitude–height structure of 40–50 day variations in atmospheric angular momentum. *J. Atmos. Sci.*, **40,** 1584–1591.

Barnett, T. P., 1985: Variations in near-global sea level pressure. *J. Atmos. Sci.*, **42,** 478–501.

Blackmon, M. L., J. E. Geisler and E. J. Pitcher, 1983: A general circulation model study of January climate anomaly patterns associated with interannual variation of equatorial Pacific sea surface temperatures. *J. Atmos. Sci.*, **40,** 1410–1425.

Boer, G. J., and N. E. Sargent, 1985: Vertically integrated budgets of mass and energy for the globe. *J. Atmos. Sci.*, **42,** 1592–1613.

Chen, S.-C., and K. E. Trenberth, 1988: Orographically forced planetary waves in the Northern Hemisphere winter: Steady state model with wave-coupled lower boundary formulation. *J. Atmos. Sci.*, **45,** 657–680.

Chen, T.-C., and W. E. Baker, 1986: Global diabatic heating during FGGE SOP-1 and SOP-2. *Mon. Wea. Rev.*, **114,** 2578–2589.

Christy, J. R., and K. E. Trenberth, 1985: Hemispheric interannual fluctuations in the distribution of atmospheric mass. *J. Geophys. Res.*, **90,** 8053–8065.

Defant, A., 1924: Die Schwankungen der atmospherischen Zirkulation uber dem Nordatlantischen Ozean im 25-jahrigne Zeitrauon 1881–1905. *Geogr. Ann.*, **6,** 13–41.

Geisler, J. E., M. Blackmon, G. T. Bates and S. Munoz, 1985: Sensitivity of January climate response to the magnitude and position of equatorial Pacific sea surface temperature anomalies. *J. Atmos. Sci.*, **42,** 1037–1049.

Holopainen, E. O., and C. Fortelius, 1986: Accuracy of estimates of atmospheric large-scale energy flux divergence. *Mon. Wea. Rev.*, **114,** 1910–1921.

Kidson, J. W., 1986: Index cycles in the Southern Hemisphere during the Global Weather Experiment. *Mon. Wea. Rev.*, **114,** 1654–1663.

Kutzbach, J. E., and R. J. Guetter, 1986: The influence of changing orbital parameters and surface boundary conditions on climate simulations for the past 18,000 years. *J. Atmos. Sci.*, **43,** 1726–1759.

Lau, K.-M., and T. J. Phillips, 1986: Coherent fluctuations of extratropical geopotential height and tropical convection in intraseasonal time scales. *J. Atmos. Sci.*, **43,** 1164–1181.

Lorenz, E. N., 1951: Seasonal and irregular variations of the Northern Hemisphere sea-level pressure profile. *J. Meteor.*, **8,** 52–59.

Madden, R. A., and P. R. Julian, 1972: Description of global-scale circulation cells in the tropics with a 40–50 day period. *J. Atmos. Sci.*, **29,** 1109–1123.

North, G. R., R. L. Bell, R. F. Cahalan and F. J. Moeng, 1982: Sampling errors in estimation of empirical orthogonal functions. *Mon. Wea. Rev.*, **110,** 699–706.

Papoulus, A., 1973: Minimum-bias windows for high-resolution spectral estimates. *IEEE Trans. Inf. Theory*, **IT-19B,** 9–12.

Rogers, J. C., and H. van Loon, 1982: Spatial variability of sea level pressure and 500 mb height anomalies over the Southern Hemisphere. *Mon. Wea. Rev.*, **110,** 1375–1392.

Rosen, R., and D. Salstein, 1983: Variations in atmospheric angular momentum on global and regional scales and the length of day. *J. Geophys. Res.*, **88,** 5451–5470.

Trenberth, K. E., 1981: Seasonal variations in global sea level pressure and the total mass of the atmosphere. *J. Geophys. Res.*, **86,** 5236–5246.

——, 1984: Interannual variability of the Southern Hemisphere circulation: Representativeness of the year of the Global Weather Experiment. *Mon. Wea. Rev.*, **112,** 108–123.

——, 1986: The signature of a blocking episode on the general circulation in the Southern Hemisphere. *J. Atmos. Sci.*, **43,** 2061–2069.

——, and J. R. Christy, 1985a: Global fluctuations in the distribution of atmospheric mass. *J. Geophys. Res.*, **90,** 8042–8052.

——, and ——, 1985b: The Southern Hemisphere circulation during FGGE and its representativeness. *Proc. of the First National Workshop on the Global Weather Experiment,* vol. 2, National Academy of Sciences, Washington DC, National Academy Press, 646–667.

——, and J. G. Olson, 1988: Intercomparison of NMC and ECMWF global analyses: 1980–1986. *NCAR* Tech. note, NCAR/TN-301 + STR, 81 pp.

——, —— and J. G. Olson, 1987: Global atmospheric mass, surface pressure and water vapor variations. *J. Geophys. Res.*, **92,** 14,815–14,826.

van Loon, H., and J. C. Rogers, 1978: The seesaw in the winter temperatures between Greenland and northern Europe. Part I: General description. *Mon. Wea. Rev.*, **106,** 296–310.

——, and R. A. Madden, 1981: The Southern Oscillation. Part I: Global associations with pressure and temperature in northern winter, *Mon. Wea. Rev.*, **109,** 1150–1162.

Walker, G. T., and E. W. Bliss, 1932: World Weather V. *Mem. Roy. Meteor. Soc.*, **4,** 53–84.

Wallace, J. M., and D. S. Gutzler, 1981: Teleconnections in the geopotential height field during the Northern Hemisphere winter. *Mon. Wea. Rev.*, **109,** 784–812.